arXiv:1603.06095v1 [cond-mat.str-el] 19 Mar 2016

Slater to Mott crossover in the metal to insulator transition of $Nd_2Ir_2O_7$

M. Nakayama,[1] Takeshi Kondo,[1,*] Z. Tian,[1] J.J. Ishikawa,[1] M. Halim,[1] C. Bareille,[1] W. Malaeb,[1,2] K. Kuroda,[1] T. Tomita,[1] S. Ideta,[3] K. Tanaka,[3] M. Matsunami,[4] S. Kimura,[5] N. Inami,[6] K. Ono,[6] H. Kumigashira,[6] L. Balents,[7] S. Nakatsuji,[1,8] and S. Shin[1]

[1]*ISSP, University of Tokyo, Kashiwa, Chiba 277-8581, Japan*
[2]*Physics Department, Faculty of Science, Beirut Arab University, Beirut, Lebanon*
[3]*UVSOR Facility, Institute for Molecular Science, Okazaki 444-8585, Japan*
[4]*Toyota Technological Institute, Nagoya 468-8511, Japan*
[5]*Graduate School of Frontier Biosciences, Osaka University, Suita, Osaka, 565-0871, Japan*
[6]*Institute of Materials Structure Science, High Energy Accelerator Research Organization (KEK), Tsukuba, Ibaraki 305-0801, Japan*
[7]*Kavli Institute for Theoretical Physics, Santa Barbara, California 93106, USA*
[8]*CREST, Japan Science and Technology Agency (JST), 4-1-8 Honcho Kawaguchi, Saitama 332-0012, Japan*

(Dated: March 22, 2016)

We present an angle-resolved photoemission study of the electronic structure of the three-dimensional pyrochlore iridate $Nd_2Ir_2O_7$ through its magnetic metal-insulator transition. Our data reveal that metallic $Nd_2Ir_2O_7$ has a quadratic band, touching the Fermi level at the Γ point, similarly to that of $Pr_2Ir_2O_7$. The Fermi node state is, therefore, a common feature of the metallic phase of the pyrochlore iridates. Upon cooling below the transition temperature, this compound exhibits a gap opening with an energy shift of quasiparticle peaks like a band gap insulator. The quasiparticle peaks are strongly suppressed, however, with further decrease of temperature, and eventually vanish at the lowest temperature, leaving a non-dispersive flat band lacking long-lived electrons. We thereby identify a remarkable crossover from Slater to Mott insulators with decreasing temperature. These observations explain the puzzling absence of Weyl points in this material, despite its proximity to the zero temperature metal-insulator transition.

The 5*d* iridium oxides (iridates), having comparable scales for their kinetic energy, coulomb interaction and spin-orbit coupling, provide an excellent platform to study new types of strongly correlated phenomena [1–11]. Amongst them, the pyrochlore iridates ($Ln_2Ir_2O_7$, where *Ln* is a lanthanide), endowed with frustrated geometry and cubic symmetry, have a particularly fascinating phase diagram. $Pr_2Ir_2O_7$, with the smallest *Ln*-ion, is a metallic spin-liquid [12–14] and exhibits an anomalous Hall effect [15, 16]. For *Ln*-ions with larger ionic radius, an antiferromagnetically ordered insulating phase appears at low temperature.

Theoretically, topological band structures have been ascribed to the $Ln_2Ir_2O_7$ series [4, 7, 17–19]. The metallic phase is predicted to exhibit quadratically dispersing conduction and valence bands touching at the Γ point close to the Fermi level (E_F) [20, 21]. This structure has been recently identified by angle-resolved photoemission spectroscopy (ARPES) in $Pr_2Ir_2O_7$ [22]. Theory predicts that such a quadratic Fermi node state may be converted into various topological states such as a topological insulator or a Weyl semimetal by appropriate symmetry breaking [4, 7, 17–19].

Antiferromagnetism in these materials is of Ising type, consisting of an "All-In-All-Out" (AIAO) configuration of Ir moments on alternating tetrahedra [24–27]. This can be considered an "octupolar" spin order which breaks time-reversal but preserves cubic symmetry, and does not enlarge the unit cell [28]. The Ising nature implies two types of domains, which have recently been shown, in agreement with theoretical predictions [29], to be separated by metallic domain walls [30, 31], which have been imaged by microwave impedence microscopy in the magnetic state of $Nd_2Ir_2O_7$ [27]. Early density functional studies predicted the magnetic state to be a Weyl semimetal [7], and general arguments imply that if a quasiparticle picture applies at low energy in the antiferromagnetic phase, and the magnetic ordering is weak, it *must* exhibit Weyl points and cannot have a true gap. Nevertheless, optical [32] and transport [30] measurements indicate a gapped insulating ground state for $Nd_2Ir_2O_7$, despite its low antiferromagnetic/Metal-Insulator (MI) transition temperature $T_{MI} \approx 30$K and proximity to metallic $Pr_2Ir_2O_7$. This begs the question of whether the weakness of the order, the quasiparticle assumption, or both, break down in this system. More generally, we seek to understand the influence of the MI transition on the conduction electrons.

In this letter, we use ARPES to investigate the evolution of the electronic structure through the MI transition in $Nd_2Ir_2O_7$, which is the most suitable member of the series for such study because its low T_c minimizes thermal broadening. Although the layered iridates have been extensively studied by photoemission [2, 33–39], ours is the first study across a MI transition in any iridate, since the latter occurs only in the pyrochlores, for which preparation of a proper crystal surface is difficult. Having overcome this challenge, we are able to directly measure both

the single particle excitations of the metallic and insulating phases. In the former, we observe features very similar to those reported for $Pr_2Ir_2O_7$ [22], indicating a quadratic band touching at the Γ point at the Fermi energy, with a valence band that is greatly narrowed (width ∼40 meV) in comparison to density functional calculations. Below T_{MI}, the band touching is removed and a gap develops. The magnitude of the gap, ∼ 40 meV, is similar to that observed in optics, and comparable to the observed bandwidth, consistent with *strong* magnetic order. These features might be understood from a Slater-type quasiparticle picture. However, we also observe that the quasiparticle peak is strongly suppressed on cooling below T_{MI}, and the valence band becomes essentially completely flat at the lowest temperature, which indicate a Mott-type insulating state with correlation-derived localization. We conclude that $Nd_2Ir_2O_7$ displays a dramatic Slater to Mott crossover with reducing temperature. This implies that Weyl fermions, if they exist, may do so only in a narrow region of temperature slightly below T_{MI}, in which the order is indeed weak and quasiparticles can survive.

Single crystals of $Nd_2Ir_2O_7$ with ∼1 mm^3 in size were grown with a flux method. The cleavage surface measured by ARPES is the (111) plane. The ARPES experiments were performed at BL7U of UVSOR facility with a MBS A-1 analyzer ($h\nu = 8 \sim 18$ eV) [40], BL28A of Photon Factory in KEK with a Scienta SES2002 analyzer ($h\nu = 39 \sim 60$ eV), and 1^3 beamline in BESSY-II with a Scienta R4000 analyzer ($h\nu = 50 \sim 60$ eV). The overall energy resolution in ARPES was set to ∼15 meV, and the lowest achievable temperature was 1K.

As previously reported, the transition temperature T_{MI} in $Ln_2Ir_2O_7$ [41] is controlled by the *Ln*-ion size [42], the pressure [42, 43], and the off-stoichiometry [44]. We have selected three pieces of $Nd_2Ir_2O_7$ crystals with different transition temperatures to investigate the variation of the MI transition with small changes in stoichiometry [30, 44, 45]. We confirmed, with an electron-probe microanalysis (EPMA), a slight deviation from stoichiometry in the Ir/Nd ratio of approximately 1% and 2% for the single crystals with zero-field T_{MI} of ∼25K and ∼20K, respectively. Figure 1 shows the resistivity, $\rho(T)$, of the crystals we used for ARPES; note that we retrieved the crystal-piece after the ARPES experiment, and measured the resistivity of exactly the same piece to properly compare the ARPES and resistivity results. The temperature derivative of $\rho(T)$, $d\rho(T)/dT$, (inset panel) enables us to estimate the value of T_{MI} from the onset of its reduction. As marked by arrows, different transition temperatures T_{MI} of ∼19K, ∼25K, and ∼36K were estimated for the three samples, which are thus labeled as MI19K, MI25K, and MI36K for the rest of the paper.

In Fig. 2, we examine the band structure in the metallic phase. Figure 2(c1) plots the typical ARPES spectra (energy distribution curves: EDCs) obtained at

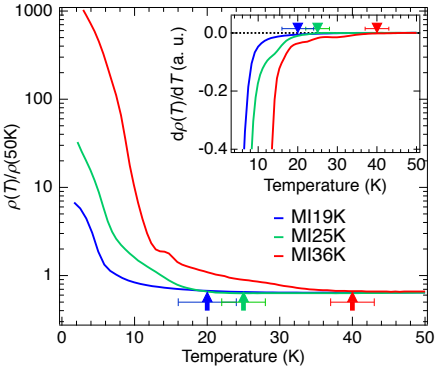

FIG. 1: (color online) Temperature dependence of the resistivity, $\rho(T)$, for $Nd_2Ir_2O_7$ crystals (MI19K, MI25K, and MI36K) we used for ARPES measurements. It is normalized to the intensity at T=50K. Inset panel plots the temperature derivative of the resistivity, $d\rho(T)/dT$. The transition temperature (T_{MI}) estimated is marked by an arrow.

(k_x, k_y)=(0,0) with low-energy photons (9.0eV ≤ $h\nu$ ≤ 11.5eV) corresponding to k_z (or $k_{(111)}$) values in the 1st Brillouin zone. Small but sharp quasiparticle peaks are observed for all of the photon energies as marked by arrows in Fig. 2(c1). We find that the quasiparticle peak approaches E_F with increasing photon energies and moves away again after getting closest to it at $h\nu$=10.5eV. In Fig. 2(c2), the EDCs are symmetrized about E_F to remove the effect of Fermi cut-off [22, 23]. We found that the gapped spectra with two peaks merge to one peak at 10.5eV, thus the band touching occurs in $Nd_2Ir_2O_7$ at the same photon energy as in $Pr_2Ir_2O_7$ [22]. To validate this further, we also used higher photon energies reaching the 3rd Brillouin zone (green circles in Fig. 2(a)), and reproduced the Fermi node again at Γ ($h\nu$=53eV) as shown in Fig. 2(d) [23].

While ARPES is a technique to observe the occupied band structure, one can visualize the unoccupied states slightly above E_F by raising the sample temperature. Figure 2(b) demonstrate such an ARPES image along a k_x cut across Γ. Here the intensities are divided by the Fermi function at the measured temperature (T=75K) to properly reveal the spectra above E_F. The spectrum becomes broad due to the short lifetime characteristic of strongly correlated systems at high temperatures, so it is not possible to detect the quasiparticle peaks in the unoccupied side. Nonetheless, significant intensities, indicative of the theoretically predicted conduction-band, are visible (a black arrow in Fig.2(b)).

Intriguingly the band width of $Nd_2Ir_2O_7$ is found to be extremely narrow, of order ∼40 meV on the occupied side, which is much less than expectated from DFT calculations. While a band narrowing is also reported for the other iridates such as Na_2IrO_3 [33], Sr_2IrO_4 [2], $Sr_3Ir_2O_7$ [34] and $SrIrO_3$ [35], it seems to be comparable or even more significant in the pyrochlore iridates,

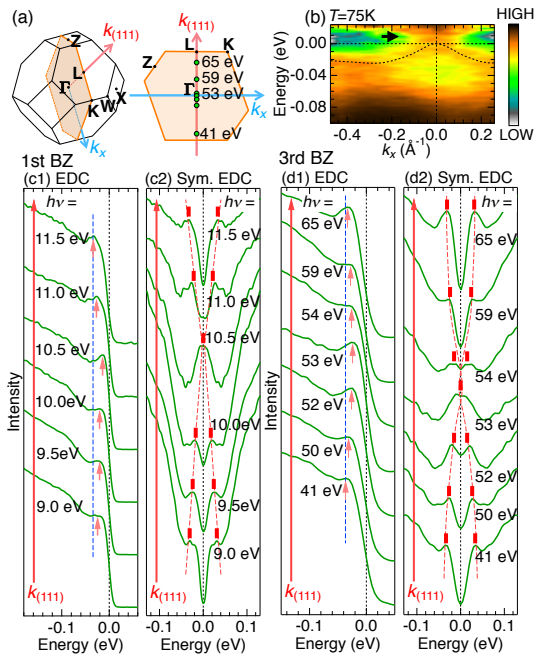

FIG. 2: (color online) (a) Brillouin zone for $Nd_2Ir_2O_7$. (b) Band dispersion map crossing Γ, divided by the Fermi function at the measured temperature (T=75K). The arrow indicates the intensities implying an expected conduction-band. EDCs (T=15K) at (k_x, k_y)=(0,0) measured with low-energy photons (c1) and high-energy photons (d1), corresponding to $k_{(111)}$s in the 1st and 3rd Brillouin zone, respectively. (c2,d2) The same data as in (c1) and (d2), respectively, but symmetrized about E_F. Arrows and bars mark peaks in the spectra.

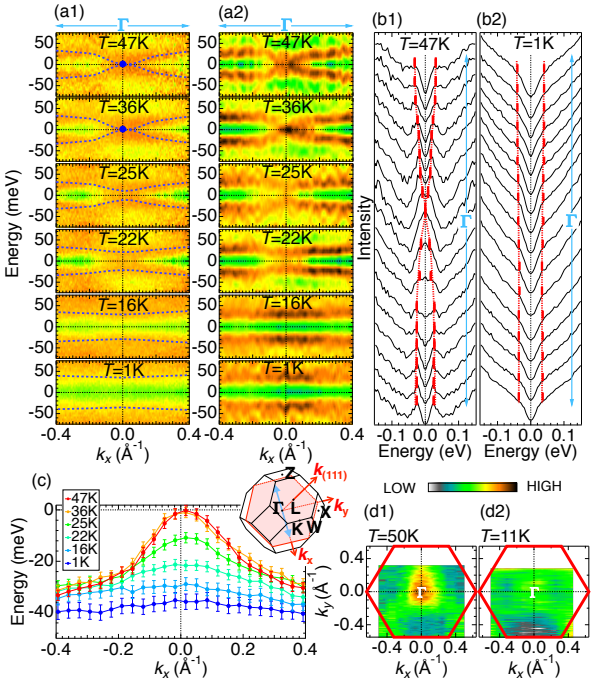

FIG. 3: (color online) (a1) Band dispersion map across Γ ($h\nu$=53eV; a light blue arrow in the inset of (c)) measured at various temperatures. The images are symmetrized about E_F. Blue dashed curves indicate the obtained band dispersions. (a2) Second derivative of the images in (a1). (b1,b2) Spectra extracted from (a1) for the metallic phase (T=47K) and the insulating phase (T=1K), respectively. (c) Temperature dependence of the band dispersion determined from the spectral peaks or shoulders (red bars in (b1) and (b2)). (d1,d2) Spectral intensities at E_F along a momentum sheet crossing Γ (red region in the inset of (c)), measured for the metallic phase ($T = 50K$) and the insulating phase (T =11K), respectively.

consistent with DMFT calculations [46]. Furthermore, we detect a peak-dip-hump structure in the spectra, as is often observed in strongly correlated systems. These results are consistent with those of $Pr_2Ir_2O_7$ [22]. The observations in both materials are consistent with a picture of the metallic state as a highly renormalized Fermi liquid [49], with small quasiparticle weight Z and large effective mass/bandwidth narrowing, for which a commensuraturely low coherence scale ϵ_{coh} of tens of meV is expected. The latter would naturally explain the strong broadening of bands at energies below ~ -0.1eV [46].

We now turn to the MI transition. In Fig. 3, we examine the temperature evolution of band dispersion through T_{MI}, measured along a momentum cut across Γ (a light blue arrow in the inset of Fig.3(c)). Figures 3(a1) and 3(a2) plot the dispersion maps for MI36K symmetrized about E_F and the 2nd derivative of those [23]. Notably the spectra above and at T_{MI} ∼36K are virtually identical, showing that there is no significant precursor of the MI transition. At temperature is dropped below T_{MI}, a gap opens at the Fermi node. This variation is also seen in the ARPES mapping at E_F along a $k_x - k_y$ sheet (red plane in the inset of Fig.3(c)); the strong intensity at Γ coming from the Fermi node (Fig. 3(d1), T=50K) vanishes below T_{MI} (Fig. 3(d2), T=11K). The band dispersion, determined from the peak/shoulder of the EDC, shown in Fig.3(c), also reflects the continuous opening of a gap below T_{MI}. These observations are consistent with a mean-field quasiparticle dispersion, in which the gap is directly controlled by the antiferromagnetic order parameter.

However, the EDCs themselves reflect strong correlations. In Figs. 3(b1) and 3(b2), the spectra for $T = 47$K and 1K corresponding to the images in Fig.3(a1) are plotted. The electronic structure in the metallic phase (Fig. 3(b1)) consists of well-defined quasiparticle peaks (red bars). In contrast, the insulating phase (Fig. 3(b2)) shows a non-dispersive flat band, and only the broad spectra lacking long-lived elections are detected, pointing to correlation-induced Mott localization. This circumstance contrasts to the insulating phase of Sr_2IrO_4 which shows relatively sharp, clearly dispersing spectra [2].

We investigate this further through the detailed vari-

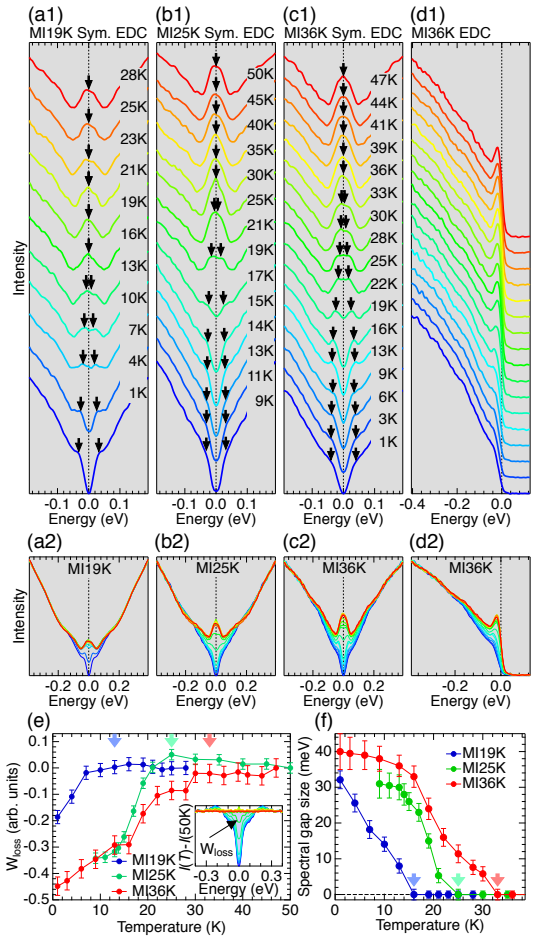

FIG. 4: (color online) (a1-c1) Temperature evolution of symmetrized EDCs for three samples (MI19K, MI25K, and MI36K) measured at the Γ point. (d1) The same data as in (c1), plotted without symmetrization. (a2-d2) The same data as in (a1-c1), but without an offset. (e) Temperature dependence of spectral wight loss near E_F (W_{loss}), which is determined to be a negative area in the difference spectra as demonstrated in the inset. (f) Temperature dependence of the magnitude of energy gap (arrows in (a1-c1)) estimated from the spectral peak positions in (a1-c1).

ation of spectral-shape at Γ. Figure 4(a1-c1) show the symmetrized EDCs from above to below T_{MI} for the three samples (MI19K, MI25K, and MI36K). In the symmetrized EDCs the gap is reflected in two split peaks (black arrows) below T_{MI}. Please note that the tracing of peak positions slightly underestimate the "real" onset temperature of gap opening, especially in 3D materials with broadened spectra due to the imperfect sample surface and k_z broadening of ARPES. Nevertheless, the persistance of quasiparticle peaks below but near T_{MI} and their shift with temperature is in accord with a Slater picture [47]. This is fully consistent with the recent discovery of an insulator to metal transition driven by external magnetic field in $Nd_2Ir_2O_7$ [30, 45], revealing that the destruction of AIAO magnetic order restores the metallic transport.

However, the data shows that the quasiparticle peak is significantly suppressed as temperature is further decreased, and it totally disappears at the lowest temperature, leaving only a broad spectrum. The abnormal variation of the quasiparticle peak is also visible in the raw EDCs (Fig. 4(d1)). While a tiny peak survives in MI19K (see Fig. 4(a1)) even at T =1K, it is attributable to small carrier doping in the insulating ground state due to the off-stoichiometry in the crystal [48]. The peak suppression is examined in Fig. 4(a2-d2) in more detail, where the spectra of Fig. 4(a1-d1) normalized to the intensities around -0.3eV are overlapped with each other. The spectral weight at E_F is gradually depleted on cooling down to the lowest temperature. This feature is more clearly demonstrated in Fig. 4(e) by plotting a spectral loss near E_F (W_{loss}) associated with the gap formation; we subtract the spectral intensities at the highest temperature from those at lower temperatures, and estimate a negative area in the difference spectra for each temperature (see the inset of Fig. 4(e)). The pseudogap-like spectral loss quantifies the crossover from the Slater-like mean field behavior near T_{MI} to the Mott regime at the lowest temperatures. The fact that the gap, extracted in Fig. 4(f), reaches ∼30-40 meV at low temperature (comparable to the optical gap [32]), is as large as the measured bandwidth, indicates the strong coupling limit, and may be responsible for this crossover.

Theory predicts that the Weyl points may migrate from the Γ point to the zone boundary and annihilate when the order parameter becomes too large [6, 18, 21], which may explain their absence in low temperature $Nd_2Ir_2O_7$. One might therefore contemplate their reappearance at intermediate temperatures just below T_{MI}, where the gap is smaller and quasiparticles are still well-defined. However, no indication of Weyl points at intermediate temperatures was found in the present ARPES measurements. Apart from the difficulty of locating incommensurate temperature-dependent features in ARPES, the progressive destruction of quasiparticles we observed may be another reason for this. We leave a dedicated search for Weyl points just below T_{MI}, perhaps using spin-resolved ARPES, for future work.

In conclusion, we carried out the first ARPES investigation of the MI transition of a three dimensional iridate. We observe a quadratic Fermi node in the metallic state of $Nd_2Ir_2O_7$ very similar to that of $Pr_2Ir_2O_7$. Upon lowering temperature below T_{MI} ∼30K, we found a drastic variation in the spectral shape, with a gradual opening of a gap and accompanying suppression of the quasiparticle peak. At the lowest achievable temperature of 1K, quasiparticles are completely suppressed and a dispersionless spectral edge is observed. The results indicate a crossover from a Slater-like mean-field effective band insulator just below T_{MI} to a Mott-like insulator with localized electrons at the lowest temperature.

We thank H. Shinaoka and E.-G. Moon for fruitful discussions and constructive comments, and D. Evtushinsky and E. Rienks for technical supports at 1^3 beamline in BESSY-II. This work was supported by JSPS KAKENHI (Nos. 24740218, 25220707, and 25707030), by the Photon and Quantum Basic Research Coordinated Development Program from MEXT, by CREST, Japan Science and Technology Agency, Grants-in-Aid for Scientific Research (No. 25707030), by Grants-in-Aids for Scientific Research on Innovative Areas (15H05882, 15H05883), and Program for Advancing Strategic International Networks to Accelerate the Circulation of Talented Researchers (No. R2604) from the Japanese Society for the Promotion of Science. L.B. is supported by DOE grant DE-FG02-08ER46524.

M. N. and T. K. contributed equally to this work.

* Electronic address: kondo1215@issp.u-tokyo.ac.jp

[1] A. T. Deller, M. Bailes, and S. J. Tingay, Science **323**, 1327 (2009).
[2] B. J. Kim *et al.*, Phys. Rev. Lett. **101**, 076402 (2008).
[3] J. Kim *et al.*, Nat. Commun. **5**, (2014).
[4] D. Pesin and L. Balents, Nat. Phys. **6**, 376 (2010).
[5] B.-J. Yang and Y. B. Kim, Phys. Rev. B **82**, 085111 (2010).
[6] W. Witczak-Krempa and Y. B. Kim, Phys. Rev. B **85**, 045124 (2012).
[7] X. Wan, A. M. Turner, A. Vishwanath, and S. Y. Savrasov, Phys. Rev. B **83**, 205101 (2011).
[8] S. Nakatsuji *et al.*, J. Phys: Conference Series. **320**, 012056 (2011).
[9] G. Jackeli and G. Khaliullin, Phys. Rev. Lett. **102**, 017205 (2009).
[10] J. Chaloupka, G. Jackeli, and G. Khaliullin, Phys. Rev. Lett. **105**, 027204 (2010).
[11] Y.-Z. You, I. Kimchi, and A. Vishwanath, Phys. Rev. B **86**, 085145 (2012).
[12] S. Nakatsuji *et al.*, Phys. Rev. Lett. **96**, 087204 (2006).
[13] Y. Tokiwa, J. J. Ishikawa, S. Nakatsuji, and P. Gegenwart, Nat. Mater. **13**, 356 (2014).
[14] D. E. MacLaughlin *et al.*, J. Phys: Conference Series. **225**, 012031 (2010).
[15] Y. Machida, S. Nakatsuji, S. Onoda, T. Tayama, and T. Sakakibara, Nature **463**, 210 (2009).
[16] L. Balicas, S. Nakatsuji, Y. Machida, and S. Onoda, Phys. Rev. Lett. **106**, 217204 (2011).
[17] B.-J. Yang and N. Nagaosa, Phys. Rev. Lett. **112**, 246402 (2014).
[18] W. Witczak-Krempa, G. Chen, Y. B. Kim, and L. Balents, Annual Review of Condensed Matter Physics **5**, 57 (2014).
[19] G. Chen and M. Hermele, Phys. Rev. B **86**, 235129 (2012).
[20] L. Savary, E.-G. Moon, and L. Balents, Phys. Rev. X **4**, 041027 (2014).
[21] E.-G. Moon, C. Xu, Y. B. Kim, and L. Balents, Phys. Rev. Lett. **111**, 206401 (2013).
[22] T. Kondo *et al.*, Nat. Commun. **6**, 10042 (2015).
[23] see Supplemental material.
[24] K. Tomiyasu *et al.*, J. Phys. Soc. Jpn. **81**, 034709 (2012).
[25] H. Guo *et al.*, Phys. Rev. B **88**, 060411 (2013).
[26] H. Sagayama *et al.*, Phys. Rev. B **87**, 100403 (2013).
[27] E. Y. Ma *et al.*, Science **350**, 538 (2015).
[28] T.-h. Arima, J. Phys. Soc. Jpn. **82**, 013705 (2013).
[29] Y. Yamaji and M. Imada, Phys. Rev. X **4**, 021035 (2014).
[30] Z. Tian *et al.*, Nat. Phys. **12**, 134 (2016).
[31] K. Ueda *et al.*, Phys. Rev. Lett. **115**, 056402 (2015).
[32] K. Ueda *et al.*, Phys. Rev. Lett. **109**, 136402 (2012).
[33] R. Comin *et al.*, Phys. Rev. Lett. **109**, 266406 (2012).
[34] P. D. C. King *et al.*, Phys. Rev. B **87**, 241106 (2013).
[35] Y. F. Nie *et al.*, Phys. Rev. Lett. **114**, 016401 (2015).
[36] Y. K. Kim *et al.*, Science **345**, 184 (2014).
[37] Y. K. Kim, N. H. Sung, J. D. Denlinger, and B. Kim, Nat. Phys. **12**, 37 (2016).
[38] A. de la Torre *et al.*, Phys. Rev. Lett. **115**, 176402 (2015).
[39] A. de la Torre *et al.*, Phys. Rev. Lett. **113**, 256402 (2014).
[40] S.-I. Kimura *et al.*, Review of Scientific Instruments **81**, 053104 (2010).
[41] K. Matsuhira, M. Wakeshima, Y. Hinatsu, and S. Takagi, J. Phys. Soc. Jpn. **80**, 094701 (2011).
[42] K. Ueda, J. Fujioka, C. Terakura, and Y. Tokura, Phys. Rev. B **92**, 121110 (2015).
[43] M. Sakata *et al.*, Phys. Rev. B **83**, 041102 (2011).
[44] J. J. Ishikawa, E. C. T. O'Farrell, and S. Nakatsuji, Phys. Rev. B **85**, 245109 (2012).
[45] K. Ueda *et al.*, Phys. Rev. Lett. **115**, 056402 (2015).
[46] H. Shinaoka, S. Hoshino, M. Troyer, and P. Werner, Phys. Rev. Lett. **115**, 156401 (2015).
[47] J. C. Slater, Phys. Rev. **82**, 538 (1951).
[48] Y. Okada *et al.*, Nature Materials **12**, 1 (2013).
[49] A "weak" non-Fermi liquid which still possesses quasiparticle peaks would also be compatible [21].

Supplemental material for Slater to Mott crossover in the metal to insulator transition of $Nd_2Ir_2O_7$

M. Nakayama,[1] Takeshi Kondo,[1,*] Z. Tian,[1] J.J. Ishikawa,[1] M. Halim,[1] C. Bareille,[1] W. Malaeb,[1,2] K. Kuroda,[1] T. Tomita,[1] S. Ideta,[3] K. Tanaka,[3] M. Matsunami,[4] S. Kimura,[5] N. Inami,[6] K. Ono,[6] H. Kumigashira,[6] L. Balents,[7] S. Nakatsuji,[1,8] and S. Shin[1]

[1]*ISSP, University of Tokyo, Kashiwa, Chiba 277-8581, Japan*
[2]*Physics Department, Faculty of Science, Beirut Arab University, Beirut, Lebanon*
[3]*UVSOR Facility, Institute for Molecular Science, Okazaki 444-8585, Japan*
[4]*Toyota Technological Institute, Nagoya 468-8511, Japan*
[5]*Graduate School of Frontier Biosciences, Osaka University, Suita, Osaka, 565-0871, Japan*
[6]*Institute of Materials Structure Science, High Energy Accelerator Research Organization (KEK), Tsukuba, Ibaraki 305-0801, Japan*
[7]*Kavli Institute for Theoretical Physics, Santa Barbara, California 93106, USA*
[8]*CREST, Japan Science and Technology Agency (JST), 4-1-8 Honcho Kawaguchi, Saitama 332-0012, Japan*

(Dated: March 22, 2016)

arXiv:1603.06095v1 [cond-mat.str-el] 19 Mar 2016

ENERGY DISTRIBUTION CURVES (EDCS) USED FOR THE SYMMETRIZATION ANALYSIS

In the main paper, we show the energy distribution curves (EDCs) symmetrized about E_F to remove the cut-off effect on the spectral shape by Fermi function. Here we present the row EDCs used for the analysis (Fig. 1).

Figure 1 shows the EDCs in the metallic phase (T=50K) of $Nd_2Ir_2O_7$, measured at various photon energies from $h\nu$ = 41 eV to 65 eV. The measured momentum cuts (dashed lines in Fig. 1(a)) are located in the $k_x - k_{(111)}$ plane crossing Γ, Z, L, and K. As marked by magenta arrows in Fig. 1(a), the quasiparticle peaks clearly disperse along k_x, and that at $k_x = 0$ (green curve in each panel) most approaches E_F at $h\nu = 53$ eV as examined in the right panel of Fig. 1(b). The symmetrized EDCs of Fig. 1(b) are plotted in Fig. 1(c). It is clearly seen that the quadratic dispersion approaches E_F with increasing the photon energy, touches E_F at $h\nu = 53$ eV, and move away from E_F again with a further increase of $h\nu$. This behavior is more clearly demonstrated in the right panel of Fig. 1(c) [same as Fig. 2(d2) in the main paper], where the curves at $k_x = 0$ are extracted.

AGREEMENT BETWEEN THE RESULTS OBTAINED WITH SYMMETRIZED SPECTRA AND FD-DIVIDED SPECTRA

In the main paper, we mainly use the symmetrization method to remove the Fermi cut-off effect from the ARPES spectra (EDCs); the EDCs are flipped about E_F and added to the original curves. This technique is widely used to visualize the opening of a gap, and also to determine the Fermi crossing point (k_F point). The method is easy to use and applicable even for the low temperature spectra with negligible intensity above E_F, thus it has been commonly used for a gap estimation in the superconducting and density-wave materials. A weakness of this method, however, is that it requires the particle-hole symmetry, and its validity is not for sure in unknown materials like $Nd_2Ir_2O_7$.

The more straightforward way of eliminating the Fermi cut-off effect would be to divide the EDCs by the Fermi function (FD) at measured temperature. For a realistic analysis, the Fermi function actually used is convoluted with the experimental energy resolution. The FD-division method, though conceptually straightforward, also has a difficulty to be applied for the data. First of all, the high temperature data are required, since it utilizes thermally populated intensities above E_F. Moreover, high quality data with a high signal/noise ratio are essential in order to reliably reproduce the spectral shape close to E_F. Therefore, the best way to extract the band dispersion close to E_F is to apply both analyses of the symmetrization and FD-division methods to the same data, and confirm a consistency between the two results.

In Fig. 2, we demonstrate that the results obtained with these two methods agree with each other, pointing to the realization of the quadratic Fermi node state in the metallic phase of $Nd_2Ir_2O_7$. Figure 2(c) plot the EDCs along a momentum cut across Γ (a light blue arrow in Fig. 2(a)). Here we use the data at T = 75K, which fulfill the following two conditions: the surviving of quasiparticles and the sufficient intensities in the thermally populated spectral weight close to E_F. The EDCs in Fig. 2(c) divided by the Fermi function and those symmetrized about E_F are exhibited in Figs. 2(d) and 2(e), respectively. The effect of Fermi cut-off near E_F is removed by these treatments, and importantly, the dispersion of spectral peaks (color bars and dashed curves) touches E_F at the Γ point in both the cases. The results are more clearly demonstrated in Fig. 2(b), where the peak positions in Figs. 2(d) and 2(e) are extracted. We find that the plots obtained by using the symmetrization

and the FD-division methods (blue and red circles, respectively) almost perfectly match with each other, both showing the Fermi node state. The consistency between the two different analyses validates our conclusion.

VARIATION OF BAND TOPOLOGY THROUGH THE METAL-INSULATOR TRANSITION

In Fig.3 of the main paper, we show the temperature evolution of band dispersion only for the sample MI36K with the highest transition temperature ($T_{\rm MI}$) of 36K among three samples we used. Here we also exhibit it for the other samples of MI19K and MI25K with the lower $T_{\rm MI}$ of 19K and 25K, respectively, and compare the results among the three samples.

Figure 3(b1) and 3(c1) show ARPES dispersion maps measured along a momentum cut across Γ (a light blue arrow in Fig. 3(a)) for MI19K and MI25K, respectively. Each image is symmetrized about E_F to visualize whether or not a gap is open. This is more clearly exhibited in Fig. 3(b2) and 3(c2), where we plot the 2nd derivative of each left image in the Figs. 3(b1) and 3(c1), respectively. The Fermi node sate with a band touching at E_F is observed in the metallic phase above $T_{\rm MI}$. Upon cooling below the $T_{\rm MI}$, the band structure becomes gapped, and the magnitude of the energy gap increases with a decrease of temperature. The band topology is eventually turned to be almost flat at the lowest temperature, meaning that the electrons are well localized with a negligible hopping. We summarize the anomalous behaviors in Figs. 3(b3) and 3(c3) by plotting the energy dispersions determined by the peak positions of spectra for MI19K and MI25K, respectively. For a comparison, we also exhibit the results of MI36K in Fig. 3(d) (same data as in Fig. 3 of the main paper). While the band topology of MI36K becomes completely flat at the lowest temperature ($T = 1$K), the weak dispersion seems to remain in MI19K and MI25K even at the lowest measured temperature. The lowest achievable temperature was only $\sim$ 10K during the experiment for MI25K conducted in BL28A of the KEK facility, hence the complete localization of electrons (or flat band) is possibly realized in the ground state of MI25K as that of MI36K. In contrast, the data for MI19K show a clear dispersion even at $T = 1$K, which is available in the 1^3 beamline of BESSY-II. This indicates that the itinerancy of conduction electrons remains in the ground state of MI19K. The relevant signature is a tiny peak surviving even at at $T = 1$K (see Fig. 4(a1)), that is the lowest achievable temperature in ARPES.

The variation in the spectral feature among crystal pieces should come from a different degree of the off-stoichiometry ($Nd_{2-x}Ir_{2+x}O_7$), which dopes a slight carrier to the crystals. In fact, the electron-probe microanalysis (EPMA) estimates the Ir/Nd ratio of approximately 1% and 2% in our single crystals with zero-field $T_{\rm MI}$ of $\sim$25K and $\sim$20K, respectively. A tiny peak observed in MI19K at $T =$1K (see Fig. 4(a1)) is therefore attributed to a small carrier doping to the Mott insulating ground state, caused by the off-stoichiometry [1].

* Electronic address: kondo1215@issp.u-tokyo.ac.jp

[1] Y. Okada *et al.*, Nature Materials **12**, 1 (2013).

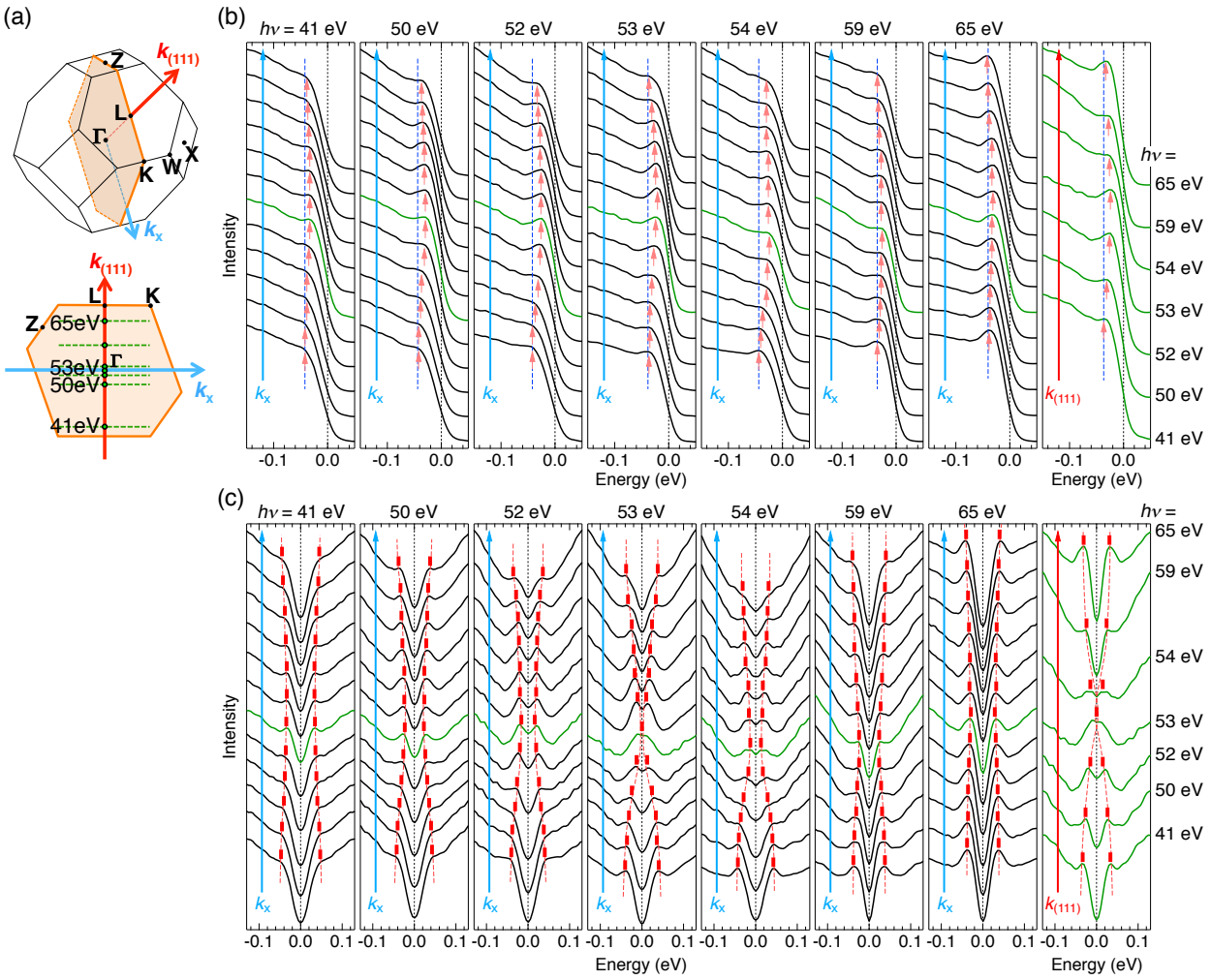

FIG. 1: (a) Brillouin zone of $Nd_2Ir_2O_7$ with measured momentum cuts at different photon energies (dashed lines). (b) EDCs measured along the k_x direction defined in (a). The used photon energies are described on top of each panel, and the corresponding momentum cuts are indicated with dashed lines in (a). On the right panel, the EDCs at k_x=0 (or along Γ-L; green circles in (a)) are extracted. The energy positions of spectral peaks are marked by arrows. The dashed blue lines are a guide to the eyes to confirm the energy dispersion in the data. (c) The symmetrized EDCs corresponding to the data in (b). The energy dispersions are indicated by red bars and dashed curves.

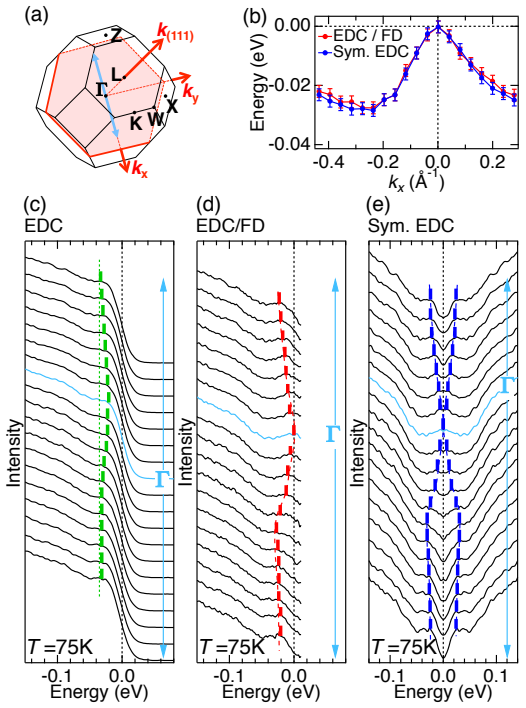

FIG. 2: (a) Brillouin zone of $Nd_2Ir_2O_7$ with the measured momentum cut crossing Γ (a light blue arrow). (b) The Fermi node state consistently obtained with two different methods: the symmetrization and the FD-division. (c) The EDCs along a momentum cut across Γ (a light blue arrow) measured at $T = 75$K. The dashed blue line is a guide to the eyes to confirm the energy dispersion in the data. (d) EDCs in (c) divided by the Fermi function at the measured temperature ($T = 75$K). (e) EDCs in (c) symmetrized about E_F. The peak energies of spectra are marked by colored bards and dashed curves.

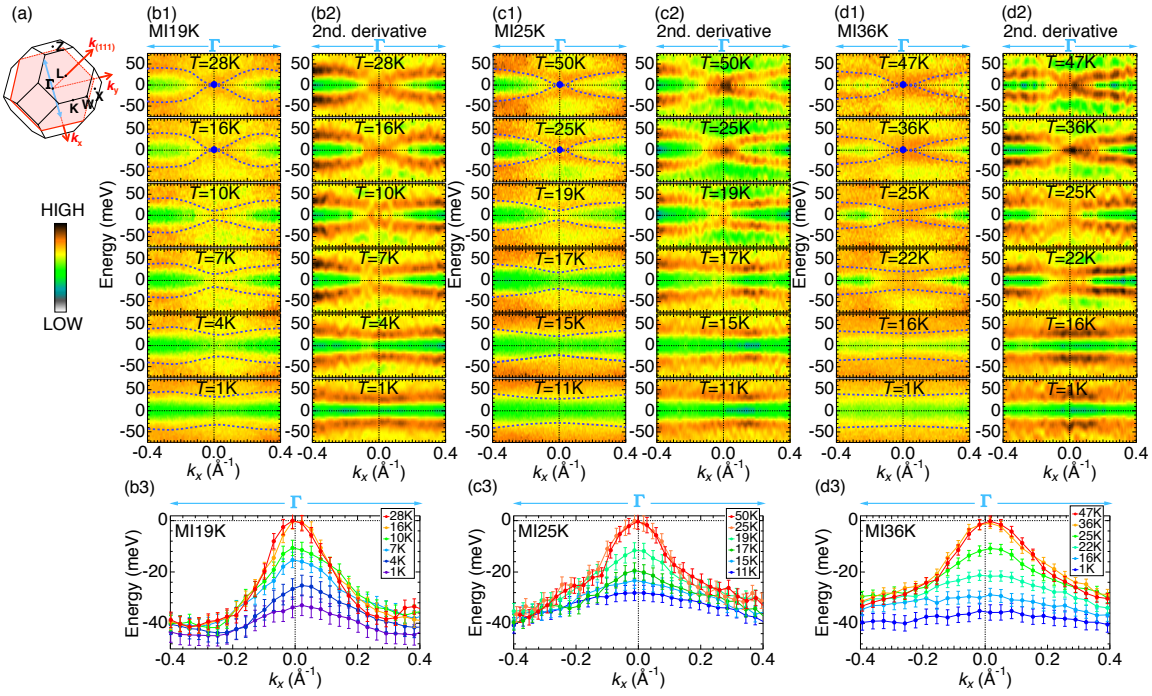

FIG. 3: (a) Brillouin zone of $Nd_2Ir_2O_7$ with the measured momentum cut crossing Γ (a light blue arrow). (b-d) Temperature evolution of ARPES dispersion measured along a momentum cut across Γ (a light blue arrow in (a)) for three samples of MI19K, MI25K, and MI36K, respectively. The left panels (b1-d1) show the ARPES images symmetrized about E_F. In the right panels (b2-d2), the 2nd derivatives of the same images as (b1-d1) are plotted. (b3-d3) The energy dispersion determined from the peak energies of spectra for MI19K, MI25K, and MI36K, respectively.